



ACOUSTICS 2012

Time-domain simulations of outdoor sound propagation: experimental validation on a complex site

D. Dagna^a, P. Blanc-Benon^a and F. Poisson^b

^aLMFA, Ecole Centrale de Lyon, 36 avenue Guy de Collongue, 69134 Ecully Cedex, France,
Metropolitan

^bInnovation et recherche SNCF, 40 avenue des terroirs de France, 75012 Paris
didier.dragna@ec-lyon.fr

Simulations of outdoor sound propagation using a time-domain approach have proved to be efficient to deal with complex situations. Indeed, the main effects on acoustic propagation can be taken into account. In particular, recent works have shown that impedance of the ground surfaces and topography can be modelled efficiently in time domain. In this paper, results from an experimental campaign carried out in la Veuve near Reims in May 2010 are compared to those obtained with a finite-difference time-domain (FDTD) solver of the linearized Euler equations. During the experiments, the topography of the site and the different surface impedances have been determined. Meteorological measurements have also been performed. A blank pistol is used to obtain impulsive signals. The different parameters are used as input into the FDTD solver. Comparisons are realized in both the frequency domain and in the time domain.

1 Introduction

Outdoor sound propagation problems are often complex. Indeed, they involve many different physical phenomena, that are due to the propagation medium and to the boundaries. Numerical simulations are then an interesting tool to model sound propagation on a realistic site. Time domain models are currently one of the most popular subject in this research field [1, 2, 3, 4].

An experimental campaign has been carried out in May 2010 on a railway site with the support of SNCF test department. An impulsive source has been used, and receivers have been set on a propagation line at different distances from the source. In this study, the waveforms and the sound pressure levels obtained experimentally are compared to those obtained with a time domain propagation model.

In the propagation model, numerical solutions of the linearized Euler equations are computed with finite-differences techniques. The model can account for:

- impedance surfaces (assuming local reaction),
- non-flat surfaces,
- mean wind and mean temperature profiles.

Impedance surfaces are taken into account through a time domain impedance boundary condition [5]. Efficient computation are obtained by using recursive convolution methods. Non-flat ground surfaces are modelled thanks to curvilinear coordinates. The propagation model has been validated with different test cases (see [6] and [7]).

In a first part, the site is described. Different parameters of the wind and temperature profiles, of the surface impedances and of the topography are presented, and are used as input data for the propagation model. In a second part, comparisons between the experimental waveforms and sound pressure levels and those obtained with the propagation model are considered.

2 Site modelling

The experimental campaign has been realized on a railway site near Reims in France in May 2010. The propagation line is perpendicular to the railway track. It is shown in Fig. 1 and Fig. 2. The origin of the cartesian coordinates is located at the center of the track, on the top of the rail and on the propagation line (see Fig. 1). The axis x coincides with the propagation line. The axis y is parallel to the railway track. The axis z is vertical.

Three receivers located at $x = 7.5$ m, $x = 25$ m and $x = 100$ m will be here considered.



Figure 1: Position of the acoustic source on the experimental site.

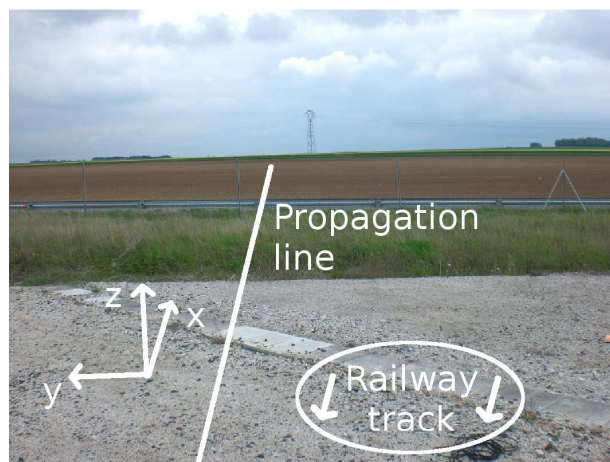


Figure 2: Propagation line considered during the experiments seen from the source.

2.1 Topography

The topography of the site has been measured along the propagation line. In the propagation model, the ground level has to be smooth, and the ground profile has been approximated by quadratic splines. Corresponding polynomial coefficients can be found in [7].

The ground profile has been plotted versus distance in Fig. 3. It is relatively flat except :

- for the ballast bed,
- near the gap around $x = 20$ m. The depth of the gap is close to 0.8 m.

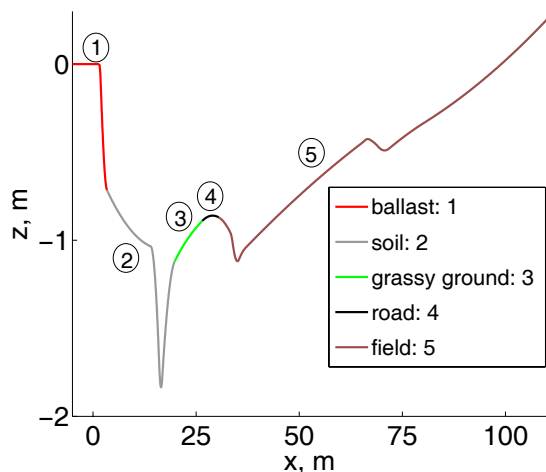


Figure 3: Topography of the experimental site implemented in the FDTD solver. The colors correspond to the different types of ground.

2.2 Ground surface impedances

Five types of ground have been distinguished. They are represented with different colors in Fig. 3. In order to get a surface impedance model for each ground, in-situ measurements using the transfer function method have been realized by l’Institut Français des Sciences et Technologies des Transports, de l’Aménagement et des Réseaux (IFSTTAR). Good fits have been obtained for the soil, the grassy ground and the field by using a one-parameter impedance model, i.e. Miki model [8]. Note that the road has been modelled by a rigid ground. Concerning the ballast bed, it has not been possible to obtain an acceptable fit with in-situ measurements. Indeed, it was complicated to account for thickness effect and to overcome multiple reflexions on the rails and on the soil. Additional measurements have been realized on the IFSTTAR’s site in Bouguenais. A good fit has been obtained by using Hamet and Bérengier impedance model [9].

Table 1: Coefficients of the surface impedance models.

	Miki			Hamet and Bérengier
	soil	grassy ground	field	ballast bed
σ_0 , kPa.s.m ⁻²	600	180	170	0.4
d , m	0.006	0.018	0.022	∞
q	-	-	-	1.4
Ω	-	-	-	0.6

The values of :

- the effective airflow resistivity σ_0 ,
- the effective thickness d ,
- the effective tortuosity q ,

- the effective porosity Ω

are given for the different grounds in Tab. 1.

2.3 Meteorological conditions

A meteorological mast has been installed on the site at $x = 125$ m near the propagation line. Three propeller anemometers and three temperature sensors have been set at heights of 1 m, 3 m and 10 m. A humidity sensor has also been installed at a height of 3 m. At last, a sonic anemometer is located at a height of 10 m.

Table 2 gives the measured values of :

- the atmospheric pressure P_0 ,
- the relative humidity r_h ,
- the temperature T_0 ,
- the sound speed c ,
- the wind speed V_0 ,
- the wind direction relative to the propagation line θ .

It should be noted that the values of V_0 and θ are averaged over one minute.

Table 2: Measured values of meteorological conditions.

z , m	P_0 , hPa	r_h , %	T_0 , °C	ρ_0 , kg.m ⁻³	c , m.s ⁻¹	V_0 , m.s ⁻¹	θ , °
1 m	991	82	6.1	1.24	-	3.3	297
3 m			6.4	1.24	-	3.5	304
10 m			6.7	1.24	335.5	4.0	315

The vertical profiles of wind and temperature are obtained with the Monin-Obukhov similarity theory. Although this theory is not applicable for inhomogeneous non-flat grounds, it allows to estimate realistic vertical profiles from a low number of measurements. A technique based on an optimisation method, and proposed by Cotté [10] is used to find the coefficients of the profiles. Figure 4 shows the vertical profiles of temperature and wind. The measurements have been made during the morning. The profiles are characteristics of an unstable atmosphere.

To obtain the sound speed profile from the temperature profile, the air is modelled as a real gas [11]. The sound speed profile is plotted versus height in Fig. 4. Note that for a height of 10 m, the value determined for c is very close to the value measured with the sonic anemometer. It should also be noticed that the atmospheric absorption is neglected in this study. Indeed, the maximal value of attenuation due to atmospheric absorption is equal to -2 dB for the receiver at $x = 100$ m and for a frequency $f = 3000$ Hz.

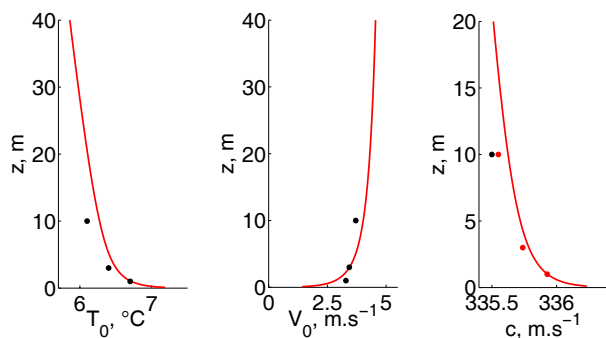


Figure 4: Vertical profiles of (left) temperature, (middle) wind speed and (right) sound speed. The black points correspond to measurements, and the red curves have been obtained by applying Monin-Obukhov similarity theory. Red points for sound speed profiles correspond to values of sound speed deduced from the temperature measurements and from the real gas model.

2.4 Source

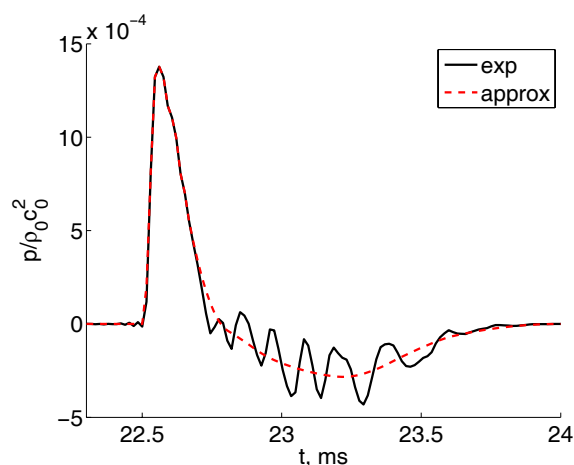


Figure 5: Example of a waveform obtained at the receiver at $x = 7.5$ m. The black and red lines correspond respectively to measurements and to the approximation.

Blank pistol shots (see Fig. 1) are used as acoustic sources. The source has been set to different heights but we consider here only a height of $z_S = 1$ m. Three shots have been fired. The directivity of the source has not been determined. Then, the source is assumed to be monopolar. The source strength $S_{\text{exp}}(f)$ can then be calculated from the waveforms. To do so, the waveform at the receiver at $x = 7.5$ m is considered, and the waveform of the direct wave is obtained by windowing the signal. In the frequency domain, the direct wave p_D can be expressed as the product of the Green function in free-field times the source strength, and:

$$p_D(\omega) = -S_{\text{exp}}(\omega) \frac{\exp(ik_{\text{eff}}R)}{4\pi R}, \quad (1)$$

where $\omega = 2\pi f$ is the angular frequency, R the distance between the source and the receiver and $k_{\text{eff}} = \omega/c_{\text{eff}}$. The term c_{eff} corresponds to the effective sound speed. An example of a waveform is shown in Fig. 5. The corresponding source strength is plotted versus frequency in Fig. 6. It can be seen that the source strength acts as a band-pass filter. The maximum is obtained at a frequency close to 900 Hz. It can also

be noted that the frequency content of the source pulse goes up to 10 kHz approximately.

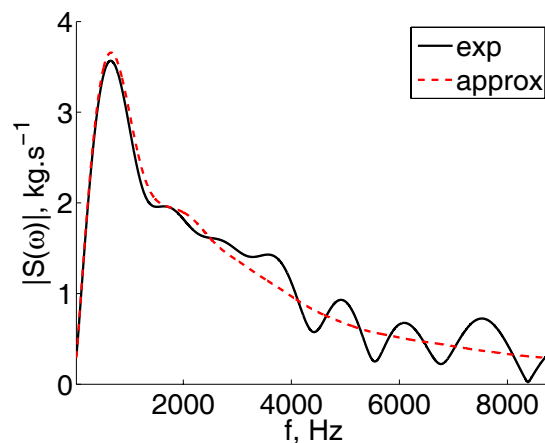


Figure 6: Source strength versus frequency. The black and red lines correspond respectively to measurements and to the approximation.

Some oscillations can be seen on the waveforms during the decompression phase. An approximation of the waveforms by quadratic splines is used to not account for these oscillations (see Fig. 5 and 6).

3 Comparison with a numerical propagation model

3.1 Description of the model

Linearized Euler equations are solved using finite-difference time-domain techniques. Surface impedances are taken into account thanks to a recursive convolution [5]. Topography is accounted for by using curvilinear coordinates [12, 6]. Details can be found in [5] and [13]. Because the geometry is invariant in the y -direction, the numerical simulation is performed in a 2-D configuration. The curvilinear coordinates are (ξ, η) . The transformation from the curvilinear coordinates system to the cartesian coordinate system is simply given by:

$$\begin{aligned} x &= \xi, \\ z &= \eta + H(x) = \eta + H(\xi), \end{aligned} \quad (2)$$

where H is the ground profile, plotted versus x in Fig. 3. The numerical domain has 11000 points in the ξ -direction and 1501 points in the η -direction. The mesh is uniform with $\Delta x = \Delta z = 0.01$ m. The CFL number defined as $\text{CFL} = c_0 \Delta t / \Delta x$ is set to 0.5. About 22 000 time iterations are calculated. The computation is performed on a vectorial machine NEC SX-8 over 8 CPU hours.

The acoustic source in the FDTD simulations is a gaussian impulsive source. The mass source term can then be written as :

$$Q(x, z, t) = \exp\left(-\frac{x^2 + (z - z_S)^2}{B^2}\right) \delta(t), \quad (3)$$

with $B = 0.06$ m. Its source strength, denoted as S_{FDTD} , is known [13]:

$$S_{\text{FDTD}}(\omega) = ik_0 \pi B^2 \exp(-k_0 B^2 / 4). \quad (4)$$

The ratio $(p/S)_{\text{FDTD}}$ is calculated from the numerical simulation and can be seen as the Green function of the problem in a 2-D geometry. A correction has to be done to account for spherical spreading. Following Parakkal *et al.* [14], the acoustic pressure in a 3-D geometry $p^{3\text{D}}$ is related to the acoustic pressure in a 2-D geometry $p^{2\text{D}}$ by:

$$p^{3\text{D}}(x, y, z) = p^{2\text{D}}(x, z) \sqrt{\frac{k_0}{2\pi i x}} \exp\left(\frac{ik_0 y^2}{2x}\right). \quad (5)$$

Comparisons in the frequency domain are then done with the ratio $p^{3\text{D}}/S$. Concerning the comparisons in the time domain, the ratio $(p^{3\text{D}}/S)_{\text{FDTD}}$ is multiplied by the source strength S_{exp} , and the numerical waveforms are obtained by an inverse Fourier transform.

At last, it should be noted that the measurements are synchronous in time. However, time at which each shot has been fired is not known. For comparison with the numerical simulation, the time origin is chosen such that the time arrival of the direct wave is the same at the receiver at $x = 7.5$ m for the numerical and experimental results.

3.2 Comparison of the results

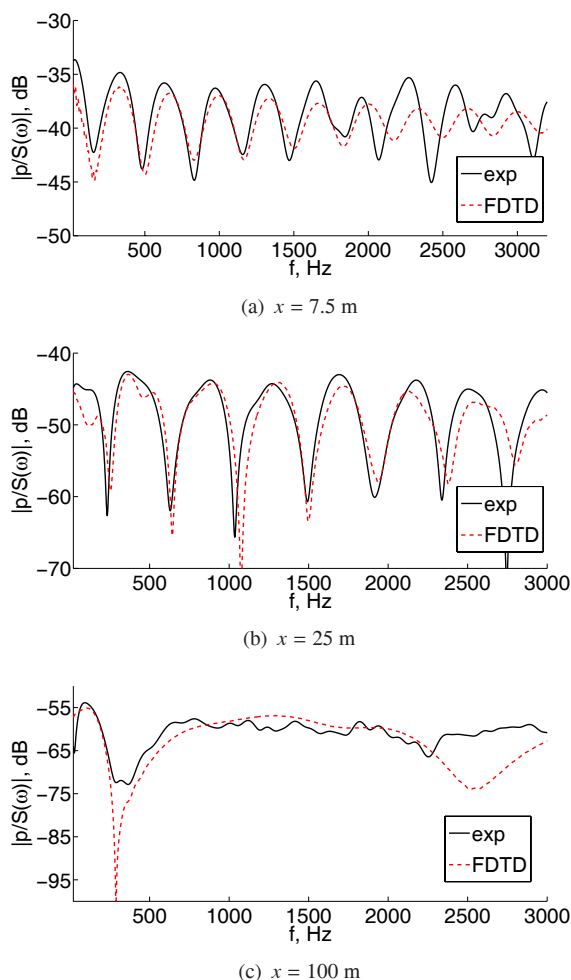


Figure 7: Sound pressure levels normalized by the source strength at receivers located at (a) $x = 7.5$ m, (b) $x = 25$ m and (c) $x = 100$ m. The height of the source is $z_s = 1$ m. — experiment and - - FDTD.

The normalized sound pressure level obtained at the three receivers with the measurements and with the numerical calculation are plotted in Fig. 7. A good agreement is globally

found. However, some discrepancies can be seen for frequencies higher than 2000 Hz.

The waveforms are plotted in Fig. 8. For the receiver at $x = 7.5$ m, the waveform obtained with the numerical simulation is similar to the measured one. It can be remarked that the shape of the waveform corresponding to the reflected wave is in close agreement with the experimental one. At the receiver at $x = 25$ m, a good matching is found. In particular, the arrival at a time $t = 80$ ms that corresponds to the wave diffracted by the gap located at $x = 20$ m is retrieved. Nevertheless, a time offset of about $\Delta t = 0.5$ ms can be observed. This can be linked to an error on the position of the source and/or of the receiver $\Delta x = c_0 \Delta t = 0.2$ m. The relative error on the time arrival is less than 1 %. At the receiver located at $x = 100$ m, the time offset is larger $\Delta t = 7$ ms. It corresponds to a relative error of about 2.5 %. However, a good agreement on the shape of the waveforms can be observed.

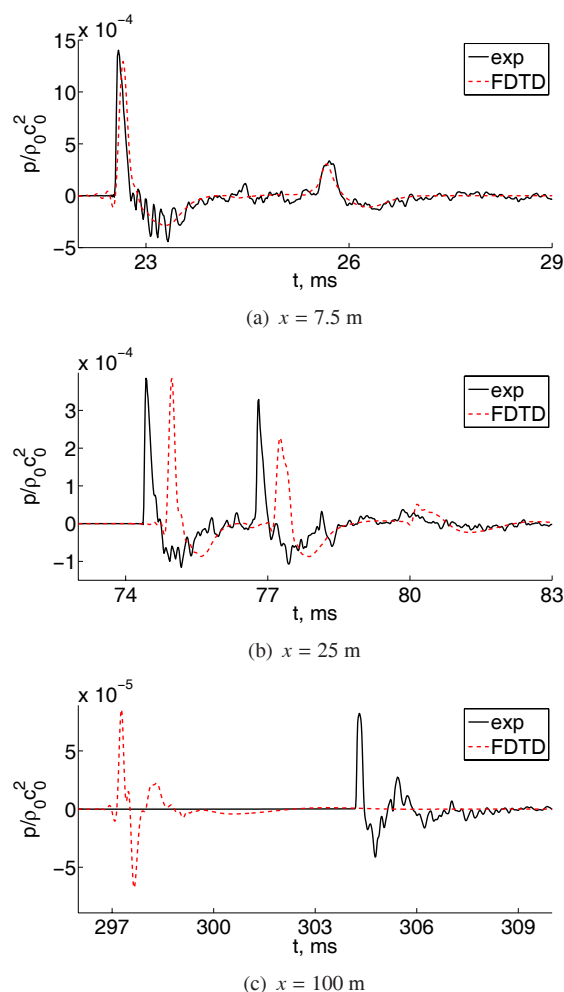


Figure 8: Pressure waveforms at receivers located at (a) $x = 7.5$ m, (b) $x = 25$ m and (c) $x = 100$ m. The height of the source is $z_s = 1$ m. — experiment and - - FDTD.

4 Conclusion

In this study, experimental results have been compared to those obtained with a time-domain propagation model. A good agreement has been obtained in the frequency domain. In the time-domain, it has been seen that the shape of the waveforms is similar. However, a time offset can be

observed. It can be linked to experimental uncertainties (position of the source and of the receivers, ...). Nevertheless, it should be noticed that the different physical phenomena are correctly taken into account in the propagation model.

It is necessary to account for more complex sources to deal with realistic transportation noise problems. The next step will be then to consider moving sources, that could be introduced on the site modelled in this study.

Acknowledgments

The authors would like to express their gratitude to Sélim Bellaj, Michel Leterrier and Sylvain Bossier from SNCF test department. Benoit Gauvreau, Philippe L'Hermite and Rémi Rouffaud from IFSTTAR are greatly acknowledged for having realized surface impedance measurements. This work was granted access to the HPC resources of IDRIS under the allocation 2011-022203 made by GENCI (Grand Equipement National de Calcul Intensif).

References

- [1] E. M. Salomons, R. Blumrich, D. Heimann, "Eulerian time-domain model for sound propagation over a finite-impedance ground surface. Comparison with frequency-domain models", *Acta Acustica United with Acustica* **88**, 483-492 (2002)
- [2] V. E. Ostashev, D. K. Wilson, L. Liu, D. F. Aldridge, N. P. Symons, D. Marlin, "Equations for finite-difference, time-domain simulation of sound propagation in moving inhomogeneous media and numerical implementation", *J. Acoust. Soc. Am.* **117**(2), 503-517 (2005)
- [3] B. Cotté, Ph. Blanc-Benon, "Time-domain simulations of sound propagation in a stratified atmosphere over an impedance ground", *J. Acoust. Soc. Am.* **125**(5), EL 202-207 (2009)
- [4] L. Ehrhardt, S. Cheinet, "Développement et évaluation d'un code de propagation acoustique en domaine temporel", 10ème Congrès Français d'Acoustique, Lyon (2010)
- [5] B. Cotté, Ph. Blanc-Benon, C. Bogey, F. Poisson, "Time-domain impedance boundary conditions for simulations of outdoor sound propagation", *AIAA J.* **47**(10), 2391-2403 (2009)
- [6] D. Dragna, Ph. Blanc-Benon, F. Poisson, "Effects of topography in time-domain simulations of outdoor sound propagation", Sixteenth AIAA/CEAS Aeroacoustics Conference, Stockholm, Suède, AIAA Paper 2010-3758 (2010)
- [7] D. Dragna, "Modélisation par une approche temporelle de la propagation acoustique en milieu extérieur : traitement de frontières complexes et validation sur site ferroviaire", Ph.D. thesis, École Centrale de Lyon n°2011-35 (2011)
- [8] Y. Miki, "Acoustical properties of porous materials - modifications of Delany-Bazley models", *J. Acoust. Soc. Jpn.* **11**(1), 19-24 (1990)
- [9] M. Bérengier, M. R. Stinson, G. A. Daigle, J.-F. Hamet, "Porous road pavement: Acoustical characterization and propagation effects", *J. Acoust. Soc. Am.* **101**(1), 155-162 (1997)
- [10] B. Cotté, "Propagation acoustique en milieu extérieur complexe : problème spécifiques au ferroviaire dans le contexte des trains à grande vitesse", Ph.D. thesis, École Centrale de Lyon n°2008-19 (2008)
- [11] O. Cramer, "The variation of the specific heat ratio and the speed of sound in air with temperature, pressure, humidity, and CO concentration", *J. Acoust. Soc. Am.* **93**(5), 2510-2516 (1993)
- [12] O. Marsden, C. Bogey, C. Bailly, "High-order curvilinear simulations of flows around non-Cartesian bodies", *J. Comp. Acoust.* **13** (4), 731-748 (2005)
- [13] D. Dragna, B. Cotté, Ph. Blanc-Benon, F. Poisson, "Time-domain simulations of outdoor sound propagation with suitable impedance boundary conditions", *AIAA J.* **49**(7), 1420-1428 (2011)
- [14] S. Parakkal, K. E. Gilbert, X. Di, H. E. Bass, "A generalized polar coordinate method for sound propagation over large-scale irregular terrain", *J. Acoust. Soc. Am.* **128**(5), 2573-2580 (2010)